MRXCAT: Realistic Numerical Phantoms for Cardiac MRI

Lukas Wissmann[1], William Paul Segars[2], and Sebastian Kozerke[1,3]

[1]*Institute for Biomedical Engineering, University and ETH Zurich, Zurich, Switzerland,* [2]*Carl E. Ravin Advanced Imaging Laboratories, Department of Radiology, The Duke University Medical Center, Durham, North Carolina, United States,* [3]*Division of Imaging Sciences & Biomedical Engineering, King's College London, London, United Kingdom*

Purpose: Image acquisition and reconstruction techniques have become a major research field over the last two decades (1,2). However, numerical simulations are often oversimplified or too specific, which compromises reproducible research. This specifically applies to cardiac MR (CMR), where motion plays a key role. The extended cardiac torso (XCAT) phantom (3) realistically models human anatomy, with options to include cardiac contraction and respiratory motion. It is the objective of the present work to propose and make available an MR extension of the XCAT phantom (MRXCAT). A simple workflow of phantom generation from the XCAT anatomy to MR raw data is implemented. Examples from cine and contrast enhanced myocardial perfusion imaging are presented. Application of the phantom to quantify errors in image reconstruction from undersampled data is demonstrated.

Methods:

MRXCAT Phantom Setup: Fig. 1 illustrates the workflow for creating a CMR numerical phantom. Anatomical masks at any spatial and temporal resolution are generated in short-axis orientation using XCAT (3). Motion parameters for both cardiac contraction and respiration can be included. The XCAT binary masks are read into Matlab (MathWorks, Natick MA, USA), which is used for all the subsequent steps. MRI contrast is mapped onto the anatomical masks by means of a signal model including sequence and tissue parameters. Various signal models are available including spoiled gradient-echo and balanced SSFP sequences. There are options to simulate dynamic contrast enhancement for first-pass perfusion imaging. Multi-coil acquisition is simulated by multiplying contrast-weighted tissue masks with coil sensitivity maps calculated using the Biot-Savart law. For this purpose, coils on circles around the chest are assumed, simulating cardiac receive coil arrays. Noise is added according to the desired signal-to-noise ratio (SNR). Optionally, the data can be gridded onto an arbitrary *k*-space trajectory including various undersampling patterns.

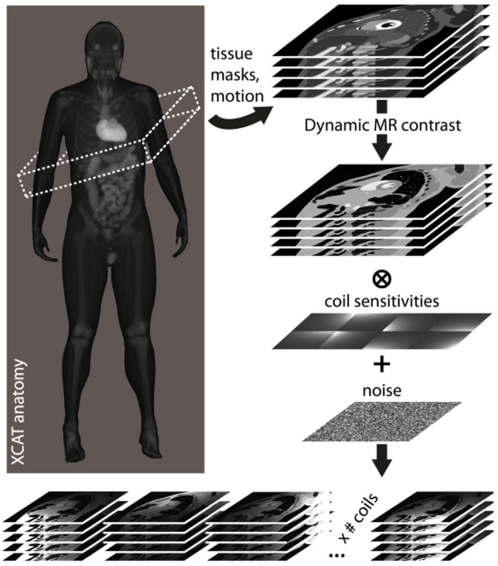

Fig. 1. MRXCAT phantom workflow. Tissue masks including motion are extracted from XCAT. MR contrast is generated for each organ. Coil sensitivities and noise are added to simulate MR acquisition.

Cine and Myocardial Perfusion Phantoms: Example phantoms for cine and myocardial perfusion imaging were generated. The heart rate was set to 63 min^{-1}, the breathing rate to 12 min^{-1}. Cine parameters included: spatial resolution = 1 mm^3, acquisition matrix = 409x400, 20 heart phases, TE = 1.5 ms, flip angle = 60°, SNR = 20. Myocardial perfusion imaging parameters were: spatial resolution = 2x2x5 mm^3, image matrix=256x210x16, 30 end-systolic time frames, contrast-to-noise ratio = 30, dynamic contrast enhancement for first-pass perfusion using a Fermi function (4).

Undersampling and Reconstruction: To demonstrate the applicability of the proposed CMR phantom to image reconstruction, accelerated 2D short-axis cine acquisition with an 8-channel receive coil with 4-fold scan acceleration was simulated. Reconstruction using SENSE (5), *k-t* PCA (6), SPARSE (7) and *k-t* SPARSE (8) was performed. Error maps in a cardiac region-of-interest (ROI) were calculated and compared to sliding window reconstruction.

Results: Fig. 2 shows different aspects of the fully sampled cine phantom. The free-breathing cine is shown in (A-B) at different inspiration states. Fig. 2(C) shows a profile along the dashed line in (B) for all heart phases of the breath-hold and free breathing case. While only cardiac contraction is visible in the breath-hold profile, both motion types appear for free breathing. A zoomed view of the heart at four heart phases is shown in (D) and all 8 coil images are presented in (E). Fig. 3 highlights specific properties of the perfusion phantom. The overview of the phantom (A) was used to mark a profile through the heart for all time frames (B). The bolus arrival in the right ventricle, left ventricle and myocardial tissue is visible. Fig. 3 (C-D) shows 2 slices of the perfusion phantom before contrast uptake and at maximum enhancement in the different cardiac compartments. In Fig. 4 the parallel imaging showcase is presented, showing a reference image and error maps for 4-fold undersampled image reconstruction. While spatiotemporal methods perform better than sliding window reconstruction, SENSE and SPARSE are inferior.

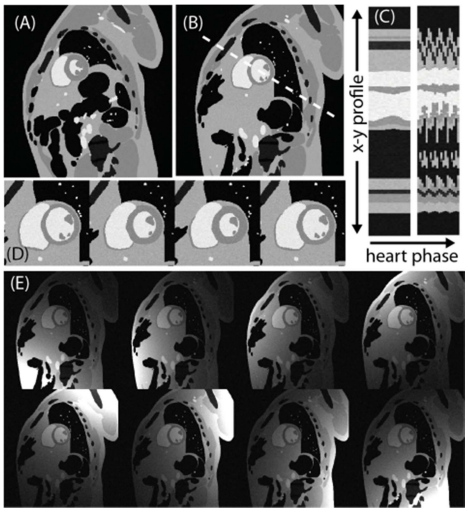

Fig. 2. 2D cine phantom. (A-B) Systole and diastole of free-breathing coil-combined image, (C) profiles along dashed line in (B) for all 20 heart phases. (D) Cardiac ROI of breath-hold cine for 4 different heart phases. (E) 8 individual coils in diastolic phase.

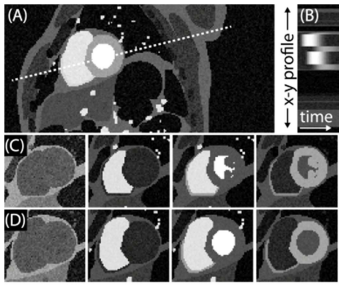

Fig. 3. Myocardial perfusion phantom. (A) Overview. (B) Slice profile vs. time along dashed line in (A). (C-D) Time frames before contrast arrival, at maximum signal in the right ventricle, left ventricle and myocardium (left-right) in 2 slices.

Discussion: In this study, a realistic numerical phantom for CMR has been introduced. The MRXCAT framework allows for versatile simulation of CMR imaging and reconstruction protocols with many degrees of freedom such as spatial and temporal resolution, noise level, number of coils and *k*-space trajectories. Specifically, the feasibility of application of the phantom to accelerated image reconstruction has been shown. Several extensions to the framework are possible. Examples include other CMR modalities, such as cardiac flow imaging or diffusion imaging.

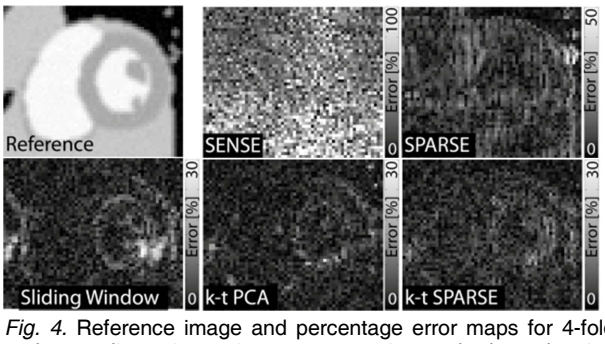

Fig. 4. Reference image and percentage error maps for 4-fold undersampling using various reconstruction methods on the cine phantom.

References: 1. Deshmane, JMRI 2012;36:55–72. 2. Tsao, JMRI 2012;36:543–560. 3. Segars, Med Phys 2010;37:4902–4915. 4. Wissmann, Proc. ISMRM 2013;21:1322. 5. Pruessmann, MRM 1999;42:952–962. 6. Pedersen, MRM 2009;62:706–716. 7. Lustig, MRM 2007;58:1182–1195. 8. Lustig, 14th Annual Meeting of ISMRM 2006:2420.